Irish Interdisciplinary Journal of Science & Research (IIJSR)
Volume 8, Issue 1, Pages 80-92, January-March 2024

Seismic Time-lapse Effects of Hydrocarbon Production on the Pressure, Porosity and Permeability Regimes in FUBA Field, Onshore Niger-Delta, Nigeria

U. Ochoma[1*]

[1]*Department of Physics, Rivers State University, P.M.B 5080, Port Harcourt, Nigeria.*
Corresponding Author Email: umaocho@gmail.com[*]

DOI: https://doi.org/10.46759/IIJSR.2024.8108

Article Received: 03 January 2024 *Article Accepted: 18 March 2024* *Article Published: 25 March 2024*

ABSTRACT

Seismic time-lapse effects of hydrocarbon production on the pressure, porosity and permeability regimes in Fuba field, onshore Niger-delta, Nigeria, are here presented, using 3D seismic time-lapse data. The Base and Monitor data have a root-mean-square repeatability ratio (RRR) of 0.38 implying a very good repeatability when considering the acquisition, processing and environmental noises. Data processing and interpretation were carried out using Petrel software. Reservoir pressure decline rate of 0.062psi/day resulted in production decline rate of 1192.21bbl/day. The structural interpretation of seismic data reveal highly synthetic and antithetic faults which are in line with faults trends identified in the Niger Delta. Three distinct horizons were mapped. Reservoir M is found at a shallower depth from 10937 to 10997 ft, reservoir N is found at a depth ranging from 11213 to 11241 ft while reservoir O is found at a deeper depth ranging from 11681 to 11871 ft respectively. The lengths, dips and orientations of the faults and horizons, in the base and monitor stacks, are not equal indicative of faults reactivation that could have resulted from hydrocarbon production. The variance edge enhanced the faults within the seismic data volume. The difference volume variance edge indicates that there are more cracks in the field of study due to production. The difference volume relative acoustic impedance indicates a reduction in porosity and permeability due to hydrocarbon production. The results of the work can be applied in the hydrocarbon exploitation scheme to minimize the damages associated with production and to ascertain reactivation of faults in the area of study.

Keywords: Seismic; Time-lapse; Hydrocarbon; Porosity; Permeability; Niger Delta; Nigeria.

1.0. Introduction

Time-lapse seismic monitoring of production-induced changes in a reservoir and the surrounding rocks over time has the basic aim of mapping reservoir compartments and subsurface rock deformation, identifying by-passed oil and pore pressure changes, monitoring fluid movement and planning for future production performance (Calvert et al., 2018; Herwanger and Koutsabeloulis, 2011; Landrø, 2001; Trani et al., 2011; MacBeth et al., 2018).

There are the technology, business and geohazard drives that may motivate a research on the effect of hydrocarbon production on surface, subsurface structures and faults reactivation using seismic time-lapse. Reservoir compaction improves production performance (Bruno, 2002; Setarri, 2002). This is possible because compaction causes reduction in porosity and permeability which affect production. Porosity loss affects the computation of oil and gas reserves (Pourciau et al., 2005). Using subsidence from time-lapse time shift, subsidence pattern may also be a good indication of permeability anisotropy and an indication of bypassed oil (Vedanti et al., 2009). Reservoir compaction can lead to reactivation of faults, casing failure and borehole breakout (Morton et al., 2006; Mildren et al., 2002).

Several researchers have made enormous contributions based on time-lapse feasibility studies and reservoir monitoring and management within the Niger Delta basin (Aniwetalu et al., 2017; Uko et al., 2018). Moreover, literatures in public domain are very scarce on seismic time-lapse, in Nigeria, with the main objective of determining effect of hydrocarbon production on subsurface structures and faults reactivation (Igwenagu, et al, 2021). Ogbamikhumi et al., 2017 evaluated the effect of changes in reservoir fluid saturations on time-lapse seismic

amplitudes. Rock physics modelling and fluid substitution studies on well logs were carried out, and acoustic impeadance change in the reservoir was estimated to be in the range of 0.25% to about 8%. Changes in reservoir fluid saturation were confirmed with time-lapse amplitudes within the crest area of the reservoir structure where porosity is 0.25%. They demonstrated the use of repeat seismic to delineate swept zones and areas hit with water override in a producing onshore reservoir. Uko and Otugo, 2016 found based only on orthometric height difference, not on reservoir stress changes that the elevation changes in this field are localized only where the measurements are located mainly in the river and drenched channels and slopes caused by erosion.

This study is taken from Fuba Field, Depobelt, Niger Delta, Nigeria. The ultimate deliverable of this study was seismic time-lapse effects of hydrocarbon production on the pressure, porosity, and permeability regimes of the area. The major components of our study are: (a) Differencing of seismic volume, (b) Well Correlation performed in order to determine the continuity of the reservoir sand across the field, (c) Seismic Interpretation which involves well-to-seismic ties, fault mapping, horizon mapping, time surface generation and attributes generation.

2.0. Location and Geology of the Study Area

The proposed study area Fuba Field is located in the onshore Niger Delta region. Figure 1 shows the map of the Niger Delta region showing the study area while Figure 2 shows the base map showing well locations in the study area.

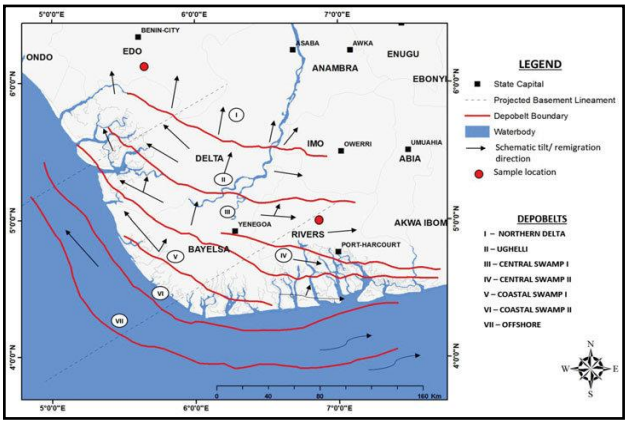

Figure 1. Map of Niger Delta Showing the study Area

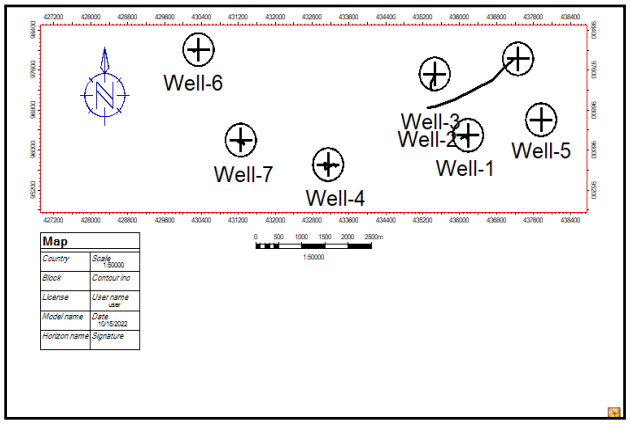

Figure 2. Base Map Showing Well Locations in the Study Area

The Niger Delta lies between latitudes 4° N and 6° N and longitudes 3° E and 9° E (Whiteman, 1982). The Delta ranks as one of the major oil and gas provinces globally, with an estimated ultimate recovery of 40 billion barrels of oil and 40 trillion cubic feet of gas (Adegoke, et al., 2017). The coastal sedimentary basin of Nigeria has been the scene of three depositional cycles (Short, and Stauble, 1967). The first began with a marine incursion in the middle Cretaceous and was terminated by a mild folding phase in Santonian time. The second included the growth of a proto-Niger delta during the Late Cretaceous and ended in a major Paleocene marine transgression. The third cycle, from Eocene to Recent, marked the continuous growth of the main Niger delta. A new threefold lithostratigraphic subdivision is introduced for the Niger delta subsurface, comprising an upper sandy Benin Formation, an intervening unit of alternating sandstone and shale named the Agbada Formation, and a lower shaly Akata

Formation. These three units extend across the whole delta and each ranges in age from early Tertiary to Recent. They are related to the present outcrops and environments of deposition. A separate member of the Benin Formation is recognized in the Port Harcourt area. It is Miocene-Recent in age with a minimum thickness of more than 6,000ft (1829m) and made up of continental sands and sandstones (>90%) with few shale intercalations (Horsfall. et al., 2017). Subsurface structures are described as resulting from movement under the influence of gravity and their distribution is related to growth stages of the delta (Ochoma, et al., 2020). Rollover anticlines in front of growth faults form the main objectives of oil exploration, the hydrocarbons being found in sandstone reservoirs of the Agbada Formation.

3.0. Methodology

3.1. Normalized Root Mean Square (NRMS) Repeatability (RRR) and Differencing of Seismic Volume

Pre-stack time migrated full-offset 3D and 4D stacks were available. The success of time-lapse reservoir monitoring depends on removing the non-repeatable effects such as configurations, seasonal changes, atmospheric temperatures, tides, elastic properties of the overburden, compaction, multiples, and rock heterogeneities (Vedanti, et al., 2009; Varela, et al., 2006). Obstructions, weather patterns, cost constraints, and maritime traffic can also influence the survey orientation. Having considered the above sources of error in repeatability, the acquisition system itself, positioning accuracy, receiver sensitivity/calibration, and source calibration must also be looked into. All these sources of error were handled through normalized root mean square (NRMS) analysis. The NRMS value is simply the RMS amplitude of the difference, normalized by the average of the RMS amplitudes of the base data and monitor data (Kragh, and Christie, 2002):

$$NRMS = -\frac{2\,rms\left(Monitor - baseline\right)}{rms\left(Monitor\right) + \left(Baseline\right)} \qquad (1)$$

$$rms = \sqrt{\frac{\sum x_i^2}{N}} \qquad (2)$$

The summation is over N number of all samples x_i (i = 1, 2, · · ·, N) in the time window.

The NRMS value is a measure of non-repeatability. If NRMS = 0, the data are perfectly repeatable. Typical “good” values of NRMS quoted in the literature range from 0.1 to 0.3 [10% to 30% non-repeatability] (Johnston, 2013).

Monitor 4D seismic volume was subtracted from the Base 3D volume, and the differences was interpreted to determine the areas of the field that have been changed during production. Areas of the field where there have been changes were analysed and compared to production activity in those areas.

3.2. Well-to-Seismic Ties

Well correlation is the first stage of the pre-interpretation process. The process of well correlation involves lithologic description, picking top and base of sand-bodies, fluid discrimination and then linking these properties from one well to another based on similarity in trends. In between these two lithologies in the subsurface, the gamma ray log is often used. Correlation of reservoir sands was achieved using the top and base of reservoir sands

picked. The correlation process was possible based on similarity in the behavior of the gamma ray log the Niger Delta; the predominant lithologies are sands and shales. In order to discriminate shapes. Also, the thickness of the shale bodies overlying and underlying the sand body is considered during Correlation. After defining the lithologies, the resistivity log was used for discriminating the type of fluid occurring within the pores in the rocks.

There are seven basic steps involved in seismic interpretation relevant to this study and they include; Differencing of seismic volume, Well-to-seismic ties, Fault Mapping, Horizon mapping, Time surface generation, Depth Conversion and attributes generation. Well-to-seismic tie is a process that enables the visualization of well information on seismic data. For this process to be achieved, the following are basic requirements; checkshot, sonic log, density log and a wavelet. The sonic log, which is the reciprocal of velocity, was calibrated using the checkshot data. The calibration process is necessary in order to improve the quality of the sonic log because the sonic log is prone to washouts and other wellbore related issues. The results of calibrating the sonic log with the checkshot gives a new log called the calibrated sonic log.

The calibrated sonic log is used along with the density log to generate an acoustic impedance (AI) log. The acoustic impedance log is calculated for each layer of rock. The next step involves generating the reflectivity coefficient (RC) log. The RC is calculated and generated using the AI log. The RC log generated is then convolved with a wavelet to generate a synthetic seismogram which is comparable with the seismic data. The statistical wavelet utilized for convolution is extracted from the seismic data. The synthetic seismogram was generated for every well that had checkshot, density and sonic log. The reflections on the synthetic seismogram were matched with the reflections on seismic data. The mathematical expressions that governs the entire well-to-Seismic tie workflow are presented below;

$$AI = \rho v \qquad (3)$$

$$RC = \frac{\rho_2 v_2 - \rho_1 v_1}{\rho_2 v_2 + \rho_1 v_1} \qquad (4)$$

$$Synthetic\ Seismogram = \frac{\rho_2 v_2 - \rho_1 v_1}{\rho_2 v_2 + \rho_1 v_1} * wavelet \qquad (5)$$

Where ρ= Density, v =Velocity, AI= Acoustic impedance and RC = Reflection coefficient

Faults were identified as discontinuities or breaks in the seismic reflections. Faults were mapped on both inline and cross-line directions. Horizons are continuous lateral reflection events that are truncated by fault lines. The horizon interpretation process was conducted along both inline and crossline direction. At the end of the horizon mapping, a seed grid is generated which serves as an input for time surface generation. Time surfaces were generated using the seed grids gotten from the horizon mapping process. The third order polynomial velocity model was generated and used to depth convert the time surfaces of the reservoirs of interest.

3.3. Variance (Edge Detection) Method

The variance attribute is edge imaging and detection techniques. It is used for imaging discontinuity related to faulting or stratigraphy in seismic data. Variance attribute is proven to help in imaging of channels, fault zones, fractures, unconformities and the major sequence boundaries (Pigott, et al, 2013). In the Petrel software, the

variance attribute uses an algorithm that computes the local variance of the seismic data through a multi-trace window with user-defined size. The local variance is computed from horizontal sub-slices for each voxel. A vertical window was used for smoothing the computed variance and the observed amplitude normalized. The variance attribute measures the horizontal continuity of the amplitude that is the amplitude difference of the individual traces from their mean value within a gliding CMP window.

$$\sigma^2 = \frac{1}{n}\sum_{f_i=1}^{n}(x_i + x_m)^2 \qquad (6)$$

Where σ = standard deviation, σ^2 = variance, n = the number of observations, f_i = frequency, x_i = the variable and x_m = mean of x_i

3.4. Dip magnitude

Dip magnitude and is analogous to strike and dip of sedimentary layers. The dip magnitude is defined as the angle between the steepest direction of a plane and a horizontal plane, where values range from 0 to 90. The dip magnitude attribute computation in Petrel software makes use of the inbuilt formula:

$$\text{True dip} = \tan^{-1}\left(\frac{\tan(\theta_y)}{\tan(\beta_x)}\right) \qquad (7)$$

where θ_y = apparent dip in a direction (y) and β_x = dip azimuth relative to a direction (x).

3.5. Determination of Relative Acoustic Impedance

The acoustic impedance inversion transforms the seismic data into an acoustic impedance model. The acoustic impedance of a media is given as equation (3). To measure acoustic impedance, it is necessary to use seismic inversion. It was assumed that the input seismic data has been processed to reduced noise and multiples, and also contains zero phase and large bandwidth. The seismic trace represents a band-limited reflective series;

$$f(t) = \frac{1}{2}\frac{\triangle\rho\upsilon}{\rho\upsilon} \qquad (8)$$

where $f(t)$ = seismic trace, $\triangle\rho\upsilon$ = the difference in the product of density and velocity. The integration of the seismic trace will provide a bandlimited estimate of the natural log of the acoustic impedance. Since the integration of band-limited, the impedance will not have absolute magnitude values and consequently is only relative. Relative acoustic impedance is an estimated inversion computed by the integration of seismic trace accompany by a high cut Butterworth zero-phase filter. It is a simplified inversion and has been generated as an asynchronous attribute in the software. It enhances acoustic impedance contrast boundaries. The relative acoustic impedance (RAI) can be computed by integrating the real part of the seismic trace (Taner, 2001).

$$\ln(\rho v) = 2\int_{t-0}^{t=1} f(T)dt \qquad (9)$$

Where $f(T)$ = real part of seismic trace. A Butterworth filter is then applied to remove long-wavelength trends that originated from the integration process (Schlumberger, 2007).

$$BL(f) = \frac{1}{1+(\frac{f}{f_H})^{2N}} \quad (10)$$

where $BL(f) =$ band –limited signal in frequency; f_H = frequency cut-off value of 10 Hz, N = filter order of 3.

It is used for delineating sequence boundaries, unconformity surfaces, and discontinuities. The acoustic impedance may be related to the formation porosity and the presence of fluid in a hydrocarbon reservoir.

4.0. Results and Discussion

4.1. Production Data

The production and reservoir pressure reports are presented in Figures 3 and 4. Production decline of 1192.21bbl/day resulted from pressure decline of 95.50bar/year or 0.062psi/year.

4.2. Normalized Root Mean Square (NRMS) Repeatability (RRR) and 4D Response

The NRMS of 0.38 has been achieved, in this study, implying very good repeatability when considering the quality of data and acquisition difference. The seismic time-lapse difference between the base and monitor surveys was successfully extracted. The fact of the difference from the monitor implies the existence of production induced effect and acquisition, environmental and processing noises, hence the 4D or time-lapse response signal (Figure 5).

4.3. Reservoir Identification, Correlation and Well-to-Seismic Ties

The results for lithology and reservoir identification are presented in Figure 6. A total of four sand bodies (L, M, N and O) were identified and correlated across all seven wells in the field. Three reservoir sands were selected for the purpose of this study (Reservoirs M, N and O). The resistivity logs which reveals the presence of hydrocarbons were used to identify the hydrocarbon bearing sands. On Figure 6, the sands are coloured yellow while shales are grey in colour. The results for well-to-seismic tie conducted on Fuba field using density log, sonic log and checkshot of Well-1 is presented in Figure 7. An extended white 2 wavelet was used to give a near perfect match between the seismic and synthetic seismogram.

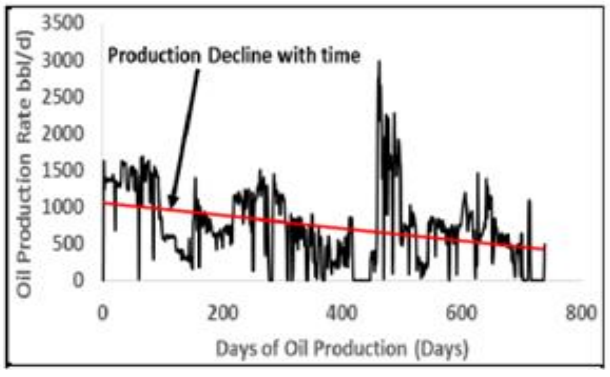

Figure 3. Reservoir Production Rate Versus Days of Oil Production

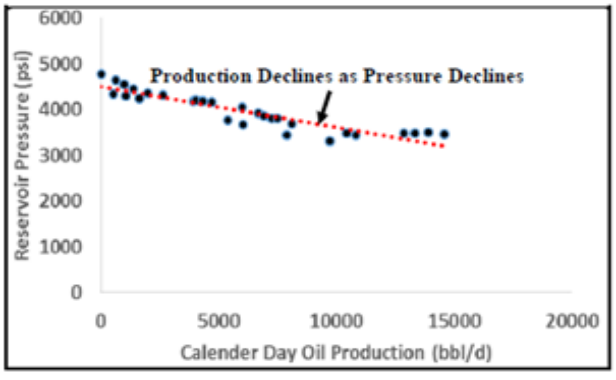

Figure 4. Effect of Reservoir Pressure Decline on Production

Irish Interdisciplinary Journal of Science & Research (IIJSR)
Volume 8, Issue 1, Pages 80-92, January-March 2024

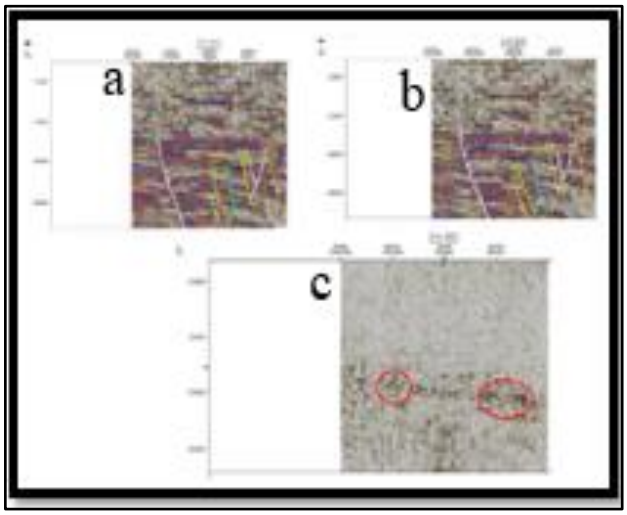

Figure 5. Base, Monitor and Difference Seismic for Inline 8590 Interpreted

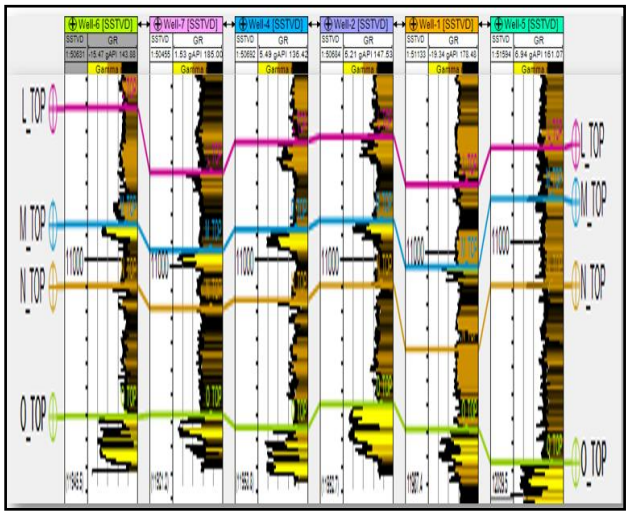

Figure 6. Well Section Showing Reservoir Section Identified and Correlated Across Fuba Field

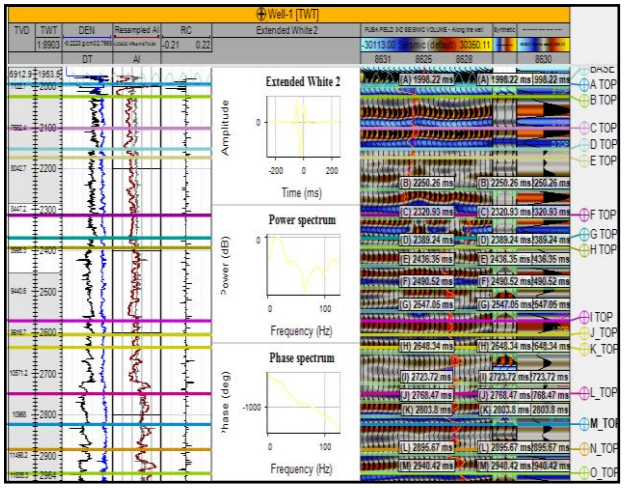

Figure 7. Synthetic Seismogram Generation and Well-to-seismic tie Conducted for Fuba Field using Well-1 Checkshot

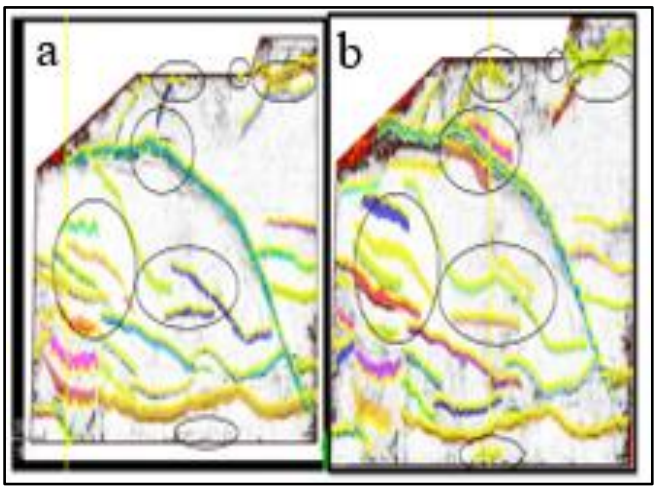

Figure 8. 4D Effect (Diffference) Betweeen Base and Monitor Interpreted Faults Displayed on the Variance Time Slice

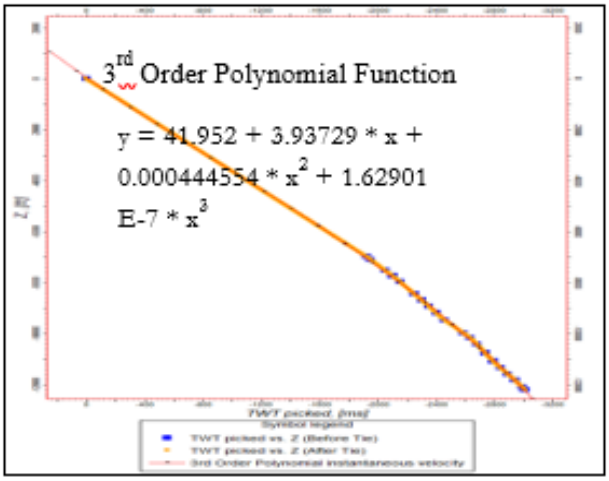

Figure 9. Third Order Polynomial Velocity model for Converting Reservoir Surfaces from Time to Depth

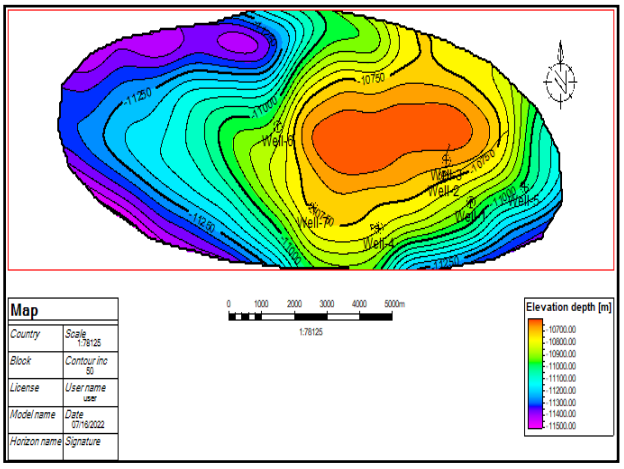

Figure 10. Reservoir Surface for Depth Surface M

Irish Interdisciplinary Journal of Science & Research (IIJSR)
Volume 8, Issue 1, Pages 80-92, January-March 2024

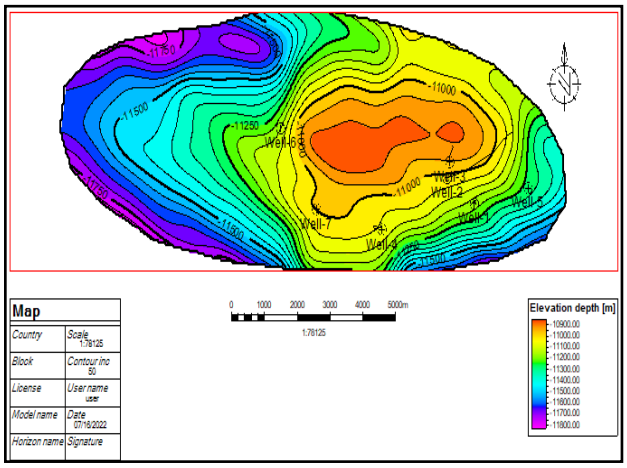

Figure 11. Reservoir Surface for Depth Surface N

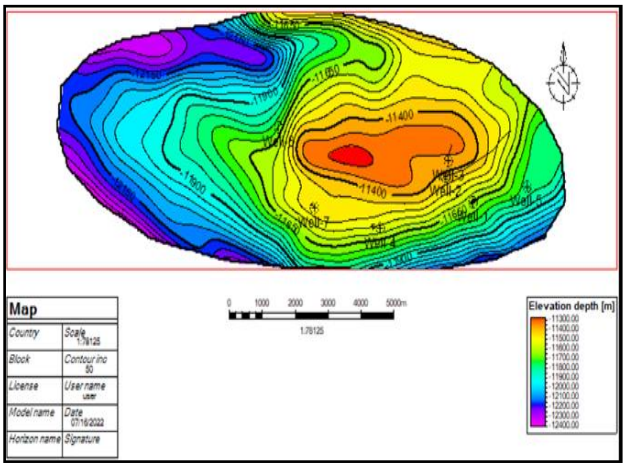

Figure 12. Reservoir Surface for Depth Surface O

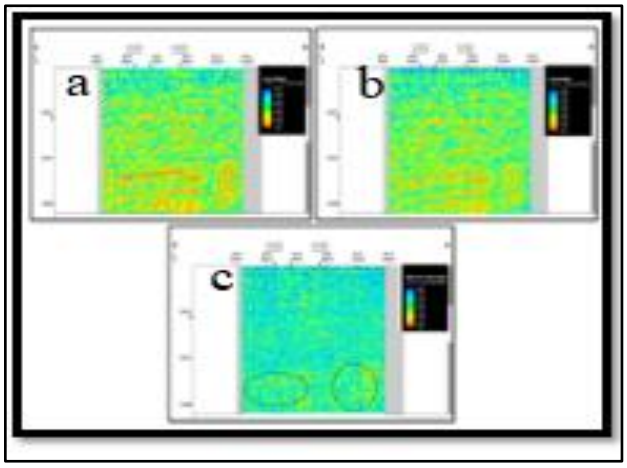

Figure 13. Dip Magnitude Inline 8515 for Base, Monitor and Difference Volume

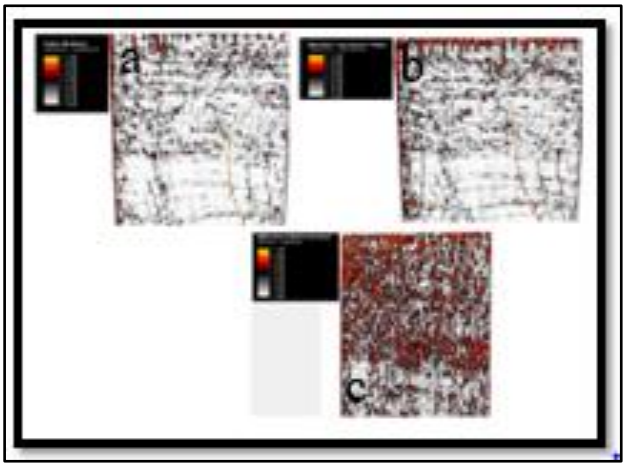

Figure 14. Variance Edge Inline 8515 for Base, Monitor and Difference Volume

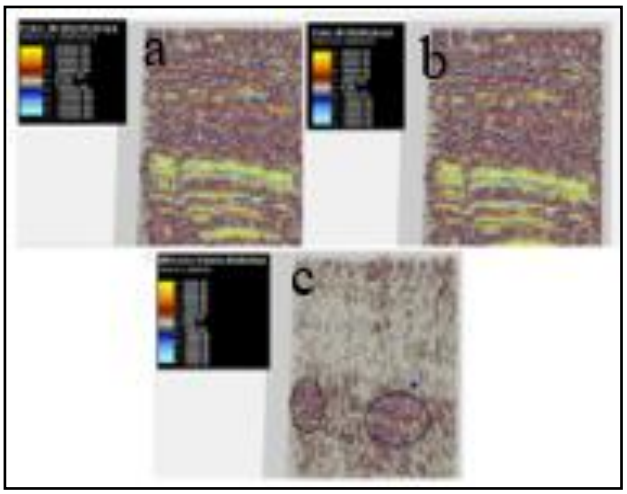

Figure 15. Relative Acoustic Impedance Inline 8515 for Base, Monitor and Difference Volume

4.4. Fault Interpretation and Structural Patterns

The results for the interpreted faults in Fuba field are presented in Figures 5 and 8. Figure 5 shows both synthetic and antithetic faults interpreted along seismic inlines for the base and monitor seismic. Faults are more visible

along the inline direction because this direction reveals the true dip position of geologic structures. Figure 5a shows the base interpreted faults, Figure 5b shows the monitor interpreted faults while Figure 5c shows the difference volume with the areas in red circles which show the 4D response. The variance time slice was used to validate the interpreted faults as seen on Figure 8. All interpreted faults are normal synthetic and antithetic faults. A total of thirty-six faults were interpreted across the entire base seismic data while a total of forty faults were interpreted across the entire monitor seismic data. Of the thirty-six interpreted faults, only F4 (synthetic fault) and F13 (antithetic fault) faults are regional, running from the top to bottom across the field for the base while only F1 (synthetic fault) and F4 (antithetic fault) faults are regional, running from the top to bottom across the field for the monitor seismic. Hence, these faults play significant roles in trap formation at the upper, middle and lower sections of the field. There is depletion of hydrostatic pressure due to production. So, areas that were cracks or fissures on the base seismic became relaxed and became well-defined or pronounced faults on the monitor seismic. In Fuba Field, the fault lengths, dips and orientations are unequal in both base and monitor seismic sections suggestive of fault reactivation from hydrocarbon production.

The results for the interpreted seismic horizons (Horizon M, Horizon N and Horizon O) are also presented in Figure 5. On these horizons, the fault polygons were generated and eliminated. The horizons were used as inputs for the generation of reservoir time surfaces. The reservoir time surfaces (M, N and O reservoirs) reveal that the reservoir structure is a collapsed crest, bounded by two regional faults (F1 and F4). Reservoir M, N and O time surfaces are truncated by two bounding faults and three minor inter-reservoir faults. The fault supported collapsed crestal structures are the closures identified on reservoir M, N and O reservoir surfaces respectively. The similarity in structure on reservoir M, N and O reveals that the field is structurally controlled by faults. The third order polynomial velocity function used for depth converting the studied surfaces is presented in Figure 9. The depth converted reservoir M, N and O surfaces are presented in Figures 10, 11 and 12 for the third order polynomial velocity function. The depth structure maps reveal that the reservoirs are anticlinal and fault supported. Reservoir M is found at a shallower depth from 10937 to 10997 ft, reservoir N is found at a depth ranging from 11213 to 11241 ft while reservoir O is found at a deeper depth ranging from 11681 to 11871 ft respectively.

4.5. Seismic Attributes

Figure 13 shows the dip magnitude of the faults for the base, monitor and difference volume. The dip magnitude values range from 0 to 90 degrees. On Figure 13, the green colors represent areas of greater dip, while the red colours represent areas of shallower dip. The dip magnitude of the faults are not equal as indicated by the difference volume (Figure 13c). This indicates that there is fault re-activation in Fuba field due to production.

Figure 14 shows the computed variance attribute of the seismic section. The range of the variance values is from 0.0 to 1.0. Discontinuities are represented by values of variance equal to 1 while the value of 0 represents a continuous seismic event. Red to yellow colourations denote the high values. There are more discontinuities in Figure 14c which implies that there are more cracks in the field of study due to production. On the variance map, the areas dotted with blue, green, orange and pink colored lines signify values that correspond to the location of the discontinuity. The discontinuities may be interpreted as faults and boundaries as shown by the lines drawn on both

attribute maps (Law and Chung, 2006). The variance edge enhanced the faults or sedimentological bodies or faults within the seismic data volume. Futhermore, high reflectivity sediments and the possibility that a potential hydrocarbon trap exists in the area are indicated by several bright spots delineated (in black circles and black ovals). Channels, fault zones, fractures, unconformities and the major sequence boundaries can be imaged using the variance attribute since it is edge imaging and detection technique. Due to similar seismic traces, there are areas with low variance values. Lineaments/discontinuities are indicated by areas with red patches while the structural framework of the field is indicated by grey areas.

The relative acoustic impedance generated in the study area is shown in Figure 15. Based on the map, the highest relative acoustic impedance is indicated by the yellow and red colours (in black circles) while the blue colour indicates the lowest relative acoustic impedance. Apparent acoustic impedance or physical property contrasts is represented by the relative acoustic impedance attribute. It is usually used for sand/shale discrimination, thickness variation and indicating sequences boundaries associated with high contrasts in acoustic impedance values, unconformity surfaces, discontinuities, porosity and hydrocarbon-bearing sand units (Oyeyemi and Aizebeokhai, 2015). Shalier facies correspond to high relative acoustic impedance values and may be interpreted as sequences boundaries while sand intervals correspond to low values (Alabi and Enikanselu, 2019). Figure 15c shows the lowest relative acoustic impedance which indicates a reduction in porosity and permeability due to hydrocarbon production.

5.0. Conclusion

Production decline of 1192.21bbl/day resulted from pressure decline of 95.50bar/year or 0.062psi/year. Most of the data points were not repeatable as evidenced in the computed Normalized root mean square (NRMS) of 0.38 meaning that on 62.0% of Base and Monitor data points were coincident. A total of four sand bodies (L, M, N and O) were identified and correlated across all seven wells in the field. Three horizons (M, N and O) were selected for the study. Reservoir M is found at a shallower depth from 10937 to 10997 ft, reservoir N is found at a depth ranging from 11213 to 11241 ft while reservoir O is found at a deeper depth ranging from 11681 to 11871 ft respectively. Structural interpretation of seismic data revealed that the field is highly faulted with synthetic and antithetic faults which are in line with faults trends identified in the Niger Delta. Fault and horizon interpretation revealed that closures found are collapsed crestal structures bounded by two major faults. The depth structure maps reveal anticlinal faults. The synthetic and antithetic faults act as good traps for the hydrocarbon accumulation in the study area. The variance edge enhanced the faults or sedimentological bodies within the seismic data volume. There are more discontinuities in the difference volume variance edge which implies that there are more cracks in the field of study due to production. The lengths, dips and orientations of the faults and horizons, in the base and monitor stacks, are not equal indicative of faults reactivation that could have resulted from hydrocarbon production. The difference volume relative acoustic impedance shows the lowest relative acoustic impedance which indicates a reduction in porosity and permeability due to hydrocarbon production. In reservoirs, hydrocarbons were encountered by all seven wells drilled in the field. Deterministic hydrocarbon volume estimation of the area of study indicates large quantities of hydrocarbon at the intervals where these structures were mapped. Within the

limits of the available data, it is recommended that further studies should include integration of stratigraphic data of all the wells. This will provide more reliable data for interpretation of the depositional environments. Also, further studies are required to confirm if these faults are sealing or leaking in which case they serve as conduits for hydrocarbon migrations rather than lateral barriers to hydrocarbon escape.

Declarations

Source of Funding

This study did not receive any grant from funding agencies in the public, commercial, or not-for-profit sectors.

Competing Interests Statement

The author declares no competing financial, professional, or personal interests.

Consent for publication

The author declares that she consented to the publication of this study.

Acknowledgements

The author is grateful to Shell Petroleum Development Company of Nigeria (SPDC), Port Harcourt Nigeria for the release of the academic data for the purpose of this study.

References

[1] Calvert, M.A., Cherrett, A.J., Micksch, U., Bourgeois, F.G., & Calvert, A.S. (2018). New Time Lapse Seismic Attribute Linking 4D and Geomechanics. 80th EAGE Conference & Exhibition, Copenhagen, Denmark, Expanded Abstracts, Pages 15–12.

[2] Herwanger, J.V., & Koutsabeloulis, N. (2011). Seismic Geomechanics: How to Build and Calibrate Geomechanical Models using 3D and 4D Seismic Data. EAGE Publications.

[3] Landrø, M. (2001). Discrimination between Pressure and Fluid Saturation Changes from Time-lapse Seismic Data. Geophysics, 66(3): 836–844.

[4] Trani, M., Arts, R., Leeuwenburgh, O., & Brouwer, J. (2011). Estimation of changes in saturation and pressure from 4D seismic AVO and time-shift analysis. Geophysics, 76: 1–17.

[5] MacBeth, C., Mangriotis, M.D., & Amini, H. (2019). Post-stack 4D Seismic Time-shifts: Interpretation and Evaluation. Geophysical Prospecting, 67: 3–31.

[6] Bruno, M. (2002). Geomechanical and Decision Analyses for Mitigating Compaction Related Casing Damage. SPE Drilling & Completion, 17(3): 179–188.

[7] Setarri, A. (2002). Reservoir compaction. Journal of Petroleum Technology, 8: 62–69.

[8] Pourciau, R., Fisk, J., Descant, F., & Waltman, R. (2005). Completion and Well Performance Results, Genesis Field, Deepwater Gulf of Mexico. SPE Drilling & Completion, 84415: 5–8.

[9] Vedanti, N., Pathak, A., Srivastava, R.P., & Dimri, V.P. (2009). Time Lapse (4D) Seismic: Some Case Studies. e-Journal Earth Science India, 2(4): 230–248.

[10] Morton, R.A., Julie, C.B., & John, A.B. (2006). Evidence of Regional Subsidence and Associated Wetland Loss Induced by Hydrocarbon Production, Gulf Coast region, USA. Environmental Geology, 50: 261–274.

[11] Mildren, S.D., Hillis, R.R., & Kaldi, J. (2002). Calibrating Predictions of Fault Seal Reactivation in the Timor Sea. Australian Petroleum Production and Exploration Association Journal, 42: 187–202.

[12] Aniwetalu, E.U., et al. (2017). Application of Time Lapse (4D) Seismic Data in Locating Hydrocarbon Prospects in Udam Field, Onshore Niger Delta, Nigeria. Journal of Petroleum and Coal, 59(5): 715–722.

[13] Uko, E.D., Famuyibo, D.A., & Okiongbo, K. (2018). Estimation of Land Surface Subsidence Induced by Hydrocarbon Production in the Niger Delta, Nigeria, using Time-Lapse Orthometric Leveling Data. Mediterranean Journal of Basic and Applied Sciences, 2(3): 1–18.

[14] Ogbamikhumi, A., Tralagba, T., & Osagiede, E.E. (2017). Time-lapse Seismic Monitoring of Offshore Reservoirs in Niger Delta, Field 'K' as a Case Study. Nigerian J. of Env. Sciences and Tech., 1(1): 23–27.

[15] Igwenagu, C.L., Uko, E.D., Tamunobereton-Ari, I., & Amakiri, A.R.C (2021). The Subsurface Structures in KOCR Field in the Niger Delta, Nigeria, Using 3d Seismic Timelapse Data. Geological Behaviour, 5(1): 7–12.

[16] Uko, E.D., & Otugo, V.N. (2016). Time-lapse Analysis of the Effects of Oil and Gas Exploitation Using Remote Sensing and GPS in Parts of the Niger Delta, Nigeria. Journal of Geography, Environment and Earth Science International, 5(4): 1–13.

[17] Whiteman, A. (1982). Nigeria: Its Petroleum Ecology Resources and Potential. London, Graham and Trotman.

[18] Adegoke, O.S., Oyebamiji, A.S., Edet, J.J, Osterloff, P.L., & Ulu, O.K. (2017). Cenozoic Foraminifera and Calcareous Nannofossil Biostratigraphy of the Niger Delta. Elsevier, Cathleen Sether, United States.

[19] Short, K.C., & Stable, A.J. (1967). Outline of Geology of Niger Delta. Bulletin of America Association of Petroleum Geologists, 51(5): 761–779.

[20] Horsfall, O.I., Uko, E.D., Tamunoberetonari I., & Omubo-Pepple, V.B. (2017). Rock-Physics and Seismic-Inversion Based Reservoir Characterization of AKOS FIELD, Coastal Swamp Depobelt, Niger Delta, Nigeria. IOSR Journal of Applied Geology and Geophysics, 5(4): 59–67.

[21] Ochoma, U., Uko, E.D., & Ayanninuola, O.S. (2020). Subsurface Structures of Onshore Fuba Field, Niger-Delta, Nigeria. International Journal of Scientific Research in Physics and Applied Sciences. 8(5): 1–5.

[22] Vedanti, N., Pathak, A., Srivastava, R.P., & Dimri, V.P. (2009). Time Lapse (4D) Seismic: Some Case Studies. e-Journal Earth Science India, 2(4): 230–248.

[23] Varela, O.J., Torres-verdin, C., Sen, M.K., & Roy, I.G. (2006). Using Time-lapse Seismic Amplitude Data to Detect Variations of ore Pressure and Fluid Saturation due to Oil Displacement by Water: A Numerical Study Based on One-dimensional Prestack Inversion. Journal of Geophysics and Engineering, 3: 177–193.

[24] Kragh, E., & Christie, P. (2002). Seismic Repeatability, Normalized Rms, and Predictability. The Leading Edge, 21(7): 640–647.

[25] Johnston, D.H. (2013). Practical Applications of Time-lapse Seismic Data. SEG Distinguished Instructor Series, 16.

[26] Pigott. J.D., Kang, M.I.H., & Han, H.C. (2013). First Order Seismic Attributes for Clastic Seismic Facies Interpretation: Examples from the East China Sea. Journal of Asian Earth Science, 66: 34–54.

[27] Taner, M.T. (2001). Seismic Attributes: Canadian Society of Exploration Geophysicists. Rec., 26(9): 48–56.

[28] Schlumberger (2007). Interpreter's Guide to Seismic Attributes. Page 115.

[29] Law W.K., & Chung A.S.C. (2006). Minimal Weighted local variance as Edge detector for active contour models. In Narayanan et al. PJ (eds.), LNCS 3851, Pages 622–632.

[30] Oyeyemi K.D., & Aizebeokhai A.P. (2015). Seismic Attributes Analysis for Reservoir Characterization; offshore Niger Delta. Journal of Petroleum and Coal, 57(6): 619–628.

[31] Alabi, A.A., & Enikanselu, P.A. (2019). Integrating Seismic Acoustic Impedance Inversion and Attributes for Reservoir Analysis Over 'DJ' Field, Niger Delta. Journal of Petroleum Exploration Production Technology, 9: 2487–2496.